

Improvements to the Analytical Linescan Model for SEM Metrology

Chris A. Mack^a, Benjamin D. Bunday^b

^aLithoguru.com, 1605 Watchhill Rd, Austin, TX 78703, E-mail: chris@lithoguru.com

^bSUNY Poly SEMATECH, Albany, NY, 12203, USA

Abstract

Critical dimension scanning electron microscope (CD-SEM) metrology has long used empirical approaches to determine edge locations. While such solutions are very flexible, physics-based models offer the potential for improved accuracy and precision for specific applications. Here, Monte Carlo simulation is used to generate theoretical linescans from single step and line/space targets in order to build a physics-based analytical model, including the presence of bottom footing and top corner rounding. The resulting analytical linescan model fits the Monte Carlo simulation results for different feature heights, widths, pitches, sidewall angles, bottom footing, and top corner rounding. This model has also been successfully applied to asymmetric features such as sidewall spacers encountered in self-aligned double patterning.

Subject Terms: Scanning electron microscope, SEM, linescan model, critical dimension, JMONSEL, CD-SEM, edge detection

1. Introduction

Scanning electron microscopes (SEMs) are frequently used to measure critical dimensions (CDs) during semiconductor integrated circuit and other nanomanufacturing. As the name implies, a SEM scans a beam of electrons across a sample and creates an image by detecting secondary electrons (secondaries) released from the sample. Analysis of a one-dimensional cut through this 2D image (called a linescan) is used to measure the width of a feature (the CD), and possibly other shape properties of the feature as well. This is a form of inverse problem, where the image of an object is given, and the desire is to “invert” the imaging process to more accurately describe the object of that image.

The inverse problem is based fundamentally on the forward problem, that is, predicting an image for a given object. For SEM imaging, this generally involves the use of a Monte Carlo simulation of electron-material interactions. In this work, the JMONSEL Monte Carlo simulator for SEM image prediction was used.¹⁻³ The nature of Monte Carlo calculations, with their random components, makes inverse calculations essentially impossible. Thus, in practice the extraction of a CD or other information about the shape of the object from a SEM image (i.e., solutions to the inverse problem) generally involves simple approaches that take little or no account of the physics of SEM image formation.⁴ Such techniques have proven mostly adequate in the past. However, as feature sizes shrink and the demands for precision and accuracy scale with those sizes, current methods may no longer suffice.^{5,6}

A different approach is model-based library matching.⁷⁻¹² In this technique, a forward-calculated imaging model is used to generate a library of simulated images over a range of expected feature types and sizes using preset materials. When an SEM image is taken from an experimental sample, it is matched and interpolated between the closest library images. While this approach can be effective, the computational burden of generating a sufficiently robust library of images is severe and matching with confidence is a challenge.

In our prior work, we have taken a somewhat intermediate path between the previously described approaches by developing a physics-inspired empirical expression for the output of an SEM called the analytical linescan model (ALM).^{13,14} The ALM is similar to the model pioneered by Frase *et al.*, who used the same basic approach adopted in this work.¹⁵ The ALM is calibrated by fitting to JMONSEL simulations of SEM images for a range of feature sizes and shapes.

In this work, the ALM is extended over a wider range of feature thicknesses, sizes, and sidewall angles, focusing on trapezoidal silicon features on a flat silicon substrate. Additionally, the impact of footing on the bottom of the trapezoid and corner rounding at the top of the trapezoid will be explored. The ALM will then be extended to asymmetrically shaped features, using sidewall spacers encountered in self-aligned double patterning (SADP) as the example.

2. Simulation of Scanning Electron Micrograph Linescans

The first step in developing a simplified analytical linescan model is to generate a series of calculated SEM images from known sample structures. Simulations of SEM images were performed using JMONSEL (Java Monte Carlo Simulator of Secondary Electrons), a program developed at the National Institute of Standards and Technology (NIST).¹⁻³ JMONSEL is used here as a “virtual SEM”, where the user can input idealized structures from a limited list of materials, with perfect user-defined geometries. The user can also define SEM parameters such as the number of incident electrons per pixel, pixel size, spot size, and beam energy. While the program can also account for charging phenomena in and around the sample and fields created by the detector, these effects were neglected in the simulations performed for this study.

In our previous study,¹⁴ the virtual samples consisted of isolated edges (steps) and line/space patterns of various sizes and pitches on a uniform substrate. Features were made of silicon on a planar silicon substrate. The sidewall angle of the edge or feature was varied between 45° and 91°. The height of the feature was varied from below 10 nm to 100 nm, though was focused on the range from 20 – 50 nm. The landing energy was set at 500 eV and a point beam of electrons was used at each pixel location (with the effect of a larger beam size to be included later). Near the line edge, a pixel size of 0.1 nm was used. The number of simulated incident electrons per pixel was between 10,000 and 25,000. An example linescan is shown in Figure 1.

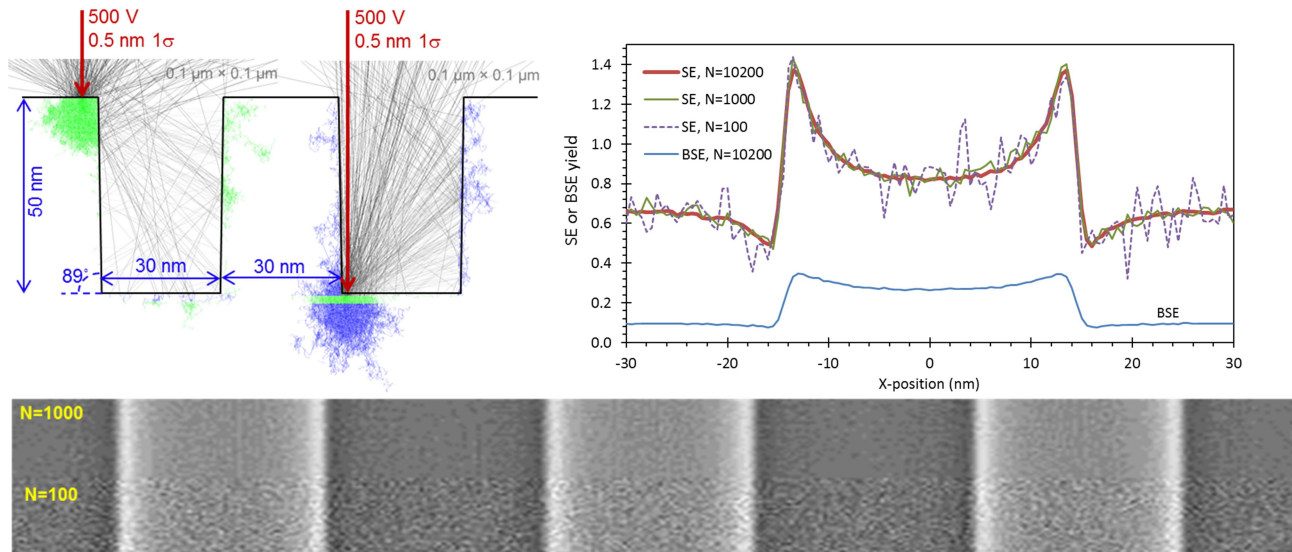


Figure 1. Example outputs from JMONSEL. Top-left: Simulated trajectories in a 30 nm line/space Si-on-thin SiO₂ structure at 500 V and 0.5 nm incident spot (one standard deviation Gaussian profile), where the interaction volumes can be seen at feature tops and bottoms. Top-right: Example linescan, including waveforms for secondary electron (SE) and backscatter electron (BSE) yields. SE electrons are defined as having energies ≤ 50 eV, with BSE electrons defined as having energies > 50 eV. Bottom: Simulated image of same waveform for N=1000 (top) and N=100 (bottom). Figure from Ref. 13.

In this work, we extend the trapezoidal feature shape by adding bottom footing and top corner rounding. As seen in Figure 2, the foot was simulated as a 2-nm tall trapezoid whose base was extended to create a “foot” of various

widths. Atop this short trapezoid was the feature trapezoid (of the same material) of height $h - 2$ nm, where h is the total feature height. Corner rounding was simulated by removing material outside of a circle of a given radius that touches both the top and sidewall of the feature. Both the bottom foot width and the top corner rounding radius were varied to see their impact on the simulated linescan and the ability of the ALM to fit those linescans.

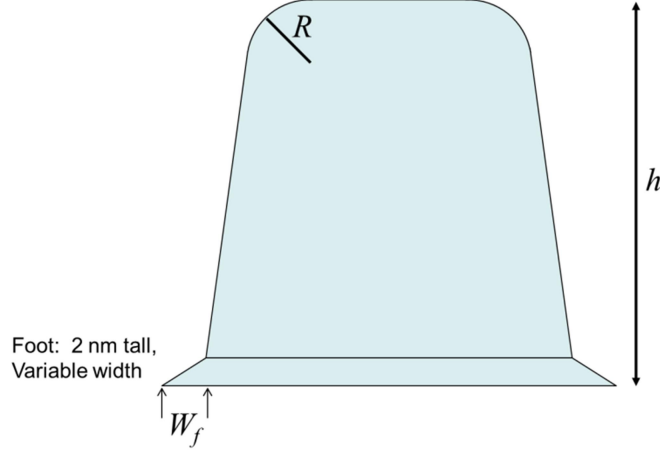


Figure 2. Geometry used to define the foot width W_f and top corner rounding radius R .

3. The Analytical Linescan Model

Our previous work derived a simple analytical linescan model.^{13,14} The linescan, corresponding to the detected secondary electrons, will be $SE(x)$, with $x = 0$ at the edge position and the feature material found at $x > 0$. For an isolated vertical edge (step), we have the following linescan expression for the case of a point incident beam:

$$SE(x) = SE(-\infty) \left[1 - \alpha_f e^{x/\sigma_f} - \alpha_b e^{x/\sigma_b} \right] u(-x) + SE(\infty) \left[1 + \alpha_e e^{-x/\sigma_e} - \alpha_v e^{-x/\sigma_v} \right] u(x) \quad (1)$$

where $u(x)$ is the unit step function. For the substrate, σ_f and σ_b are the forward and backscatter ranges, respectively, within the substrate material, α_f is the fraction of substrate forward scatter-generated secondaries absorbed by the step, and α_b is the fraction of substrate backscatter-generated secondaries absorbed by the step. When the electron beam is incident on the top of the step, σ_e is the forward scatter range of the step material and α_e is the fraction of those forward-scattered electrons that escape through the edge of the step. When the incident beam is very close to the step, however, the interaction volume of the forward-scattered electrons with the material is reduced, causing the generation of less secondaries. Thus, we subtract a term $\alpha_v e^{-x/\sigma_v}$ to account for this volume loss where $\sigma_v < \sigma_e$. $SE(-\infty)$ is the secondary electron signal for the substrate a long way from any feature, and $SE(\infty)$ is the secondary electron signal for the top of the step a long way from the step edge. For the case of a silicon step on a silicon wafer, these two values will be the same.

For the case of a sloped step, a sloped region of width $h/\tan\theta$ exists between the top and bottom of the step, where θ is the sidewall angle. If the width of the sloped region is sufficiently large, the middle of the sidewall region has a steady secondary electron signal, which we will call SE_{edge} . This signal level then falls to the bottom level over a characteristic distance δ_1 at the bottom of the step, and rises to the top level over a characteristic distance δ_2 at the top of the step, forming an S-shaped waveform. The model for the linescan in this sloped region is

$$c_1 = SE(-\infty) \left[1 - \alpha_f - \alpha_b \right] - SE_{edge}$$

$$SE(x) = SE_{edge} + \left(c_1 - c_2 e^{-(h/\tan\theta)/\delta_2} \right) e^{-x/\delta_1} + \left(c_2 - c_1 e^{-(h/\tan\theta)/\delta_1} \right) e^{-(h/\tan\theta-x)/\delta_2} \quad (2)$$

Many of the model parameters used in the above two equations are a function of the sidewall angle, and a few are a function of step height. Letting \tilde{p} represent the value of a parameter p for a 90° step, the variation of the linescan parameters with sidewall angle and feature height for the case of silicon features on a silicon wafer take the forms

$$\begin{aligned} \sigma_b &= s_b h \\ \alpha_f &= \tilde{\alpha}_f + 0.218 \cos \theta - 0.375 \cos^2 \theta \\ \alpha_b &= \tilde{\alpha}_b (1 - \cos \theta)^2 \\ \sigma_e &= \sigma_f + (\tilde{\sigma}_e - \sigma_f) (1 - \cos \theta)^2 \\ \alpha_e &= \tilde{\alpha}_e (1 - \cos \theta) \\ \alpha_v &= -0.08 + (\tilde{\alpha}_v + 0.08) e^{-9.43 \cos \theta} \\ SE_{edge} &= \tilde{SE}_{edge} (1 + 1.11 \cos \theta - 4.08 \cos^2 \theta + 2.75 \cos^3 \theta) \\ \delta_1 &= 4.0 (1 - e^{-1.02 \cos \theta}) \\ \delta_2 &= \left(\frac{H}{135} \right)^2 + 1.2 \cos \theta \end{aligned} \quad (3)$$

where all dimensions are in nanometers. Further, these equations only apply to the case where $h \geq 20$ nm. The values of the parameters for a 90° sidewall angle are given in Table I.

Table I. Best fit parameters to rigorous Monte Carlo simulations of an isolated silicon step on a silicon wafer at 500 V electron landing voltage.

	Silicon Step
Si wafer background signal, $SE(-\infty)$	0.817
Si wafer forward scatter range, σ_f (nm)	1.95
Si wafer backscatter range per step height, $s_b = \sigma_b/h$	0.82
Si wafer forward scatter absorption, $\tilde{\alpha}_f$	0.245
Si wafer backscatter absorption, $\tilde{\alpha}_b$	0.22
Step sidewall signal, \tilde{SE}_{edge}	1.52
Step forward scatter range, $\tilde{\sigma}_e$ (nm)	2.66
Step volume loss range, σ_v (nm)	0.26
Step edge enhancement factor, $\tilde{\alpha}_e$	1.65
Step volume loss factor, $\tilde{\alpha}_v$	0.64
Step background signal, $SE(\infty)$	0.817

Real scanning electron microscopes do not have point beams of electrons impinging on the sample. Instead, the beam is approximately a Gaussian owing to the finite resolution of the microscope and other beam non-idealities. Thus, the expected linescan will be the point linescan model (equations (1) and (2) combined) convolved with a Gaussian.¹⁴

A feature such as a line or a space can be constructed as the combination of two edges, using the ALM for an edge defined in the previous section. However, small spaces act as traps for escaping secondary electrons, so that some of the model parameters must be modified as a function of the size of the space. In the region of the space, the result is that smaller spaces have smaller forward scatter absorption and larger backscatter absorption.

$$\alpha_f = \tilde{\alpha}_f \left(1 - e^{-(s/(0.65h))^{1.3}} \right), \quad \alpha_b = \tilde{\alpha}_b \left(1 + 1.35e^{-(s/h)} \right) \quad (4)$$

where s is the spacewidth. Likewise, when the electron beam scan across the top of the feature, secondaries escaping out of the edge of the feature are more likely to be trapped in the space, causing a reduction in both the step edge enhancement factor and the step volume loss factor.

$$\alpha_e = \tilde{\alpha}_e \left(1 - e^{-(s/(0.93h))^{0.62}} \right), \quad \alpha_v = \tilde{\alpha}_v \left(1 - e^{-(s/(0.5h))^{0.5}} \right) \quad (5)$$

Figure 3 shows an example where all of these factors are taken into account. The ALM prediction matches the Monte Carlo simulations extremely well. And while the example given is for a point beam of electrons, the use of a Gaussian beam incident on the sample does not pose any particular challenges and does not reduce the quality of the match to the Monte Carlo results.

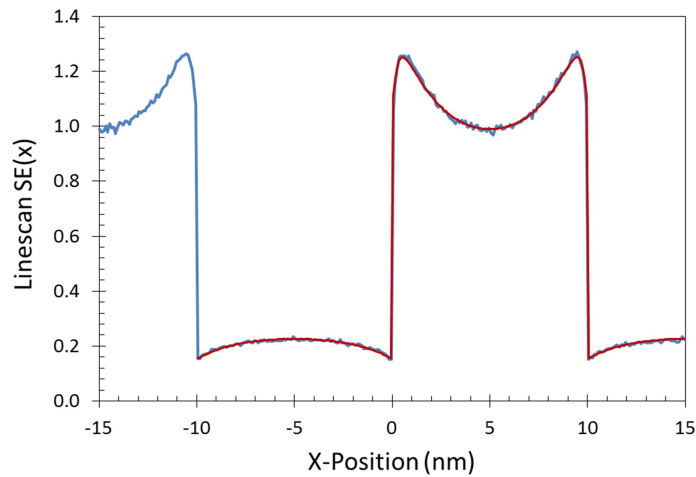


Figure 3. The ALM (red smooth curve) compared to the Monte Carlo simulation results (blue jagged curve) for 30-nm tall silicon features on a silicon wafer, SWA = 90°, 10-nm lines and spaces (RMS error = 0.0075).

4. Adding Footing and Top Corner Rounding to the ALM

So far, all features incorporated into the ALM have been trapezoids. JMONSEL was also used to simulate the impact of bottom footing and top corner rounding on the linescans, varying both the width of the foot and top corner rounding radius up to 10 nm. Figure 4 shows the impact of a small foot. For the no-foot case, the sharp minimum of the linescan corresponds to the bottom corner of the trapezoid. Adding a 1-nm wide foot moves this minimum by 1 nm,

but also increases the *SE* signal of that minimum (Fig. 4a). As the length of the foot grows, the minimum corresponding to the outside edge of the foot becomes less distinct. Just as the position of the bottom of the feature becomes indistinct in the presence of a foot, the position of the linescan minimum becomes correspondingly less distinct. From the perspective of the ALM, the presence of a foot a few nanometers in length or longer is about equivalent to making $\alpha_f \approx 0$. If the goal of using the ALM is to shed light on the width of the feature (that is, ignoring the foot), then setting $\alpha_f \approx 0$ is probably sufficiently accurate.

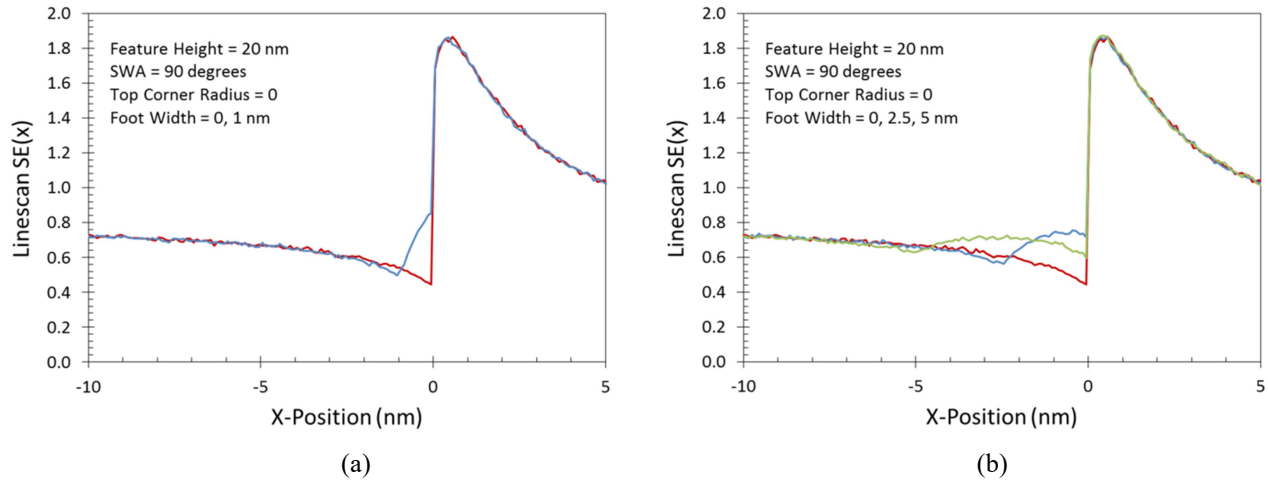


Figure 4. Monte Carlo simulation results showing the impact of a 2-nm tall trapezoidal foot of varying widths on the resulting linescan (20-nm tall, 90° silicon edge on a silicon wafer, 500 V, point beam of electrons). The linescans with and without a foot are compared for (a) a 1-nm wide foot, and (b) a 2.5-nm and 5-nm foot.

Rounding the top corner of the trapezoidal feature impacts the linescan as shown in Figure 5. There are three distinct impacts of top corner rounding. First, the position of the peak, which corresponds to the sharp top corner of the trapezoid, moves to the left as that corner becomes rounded. This is equivalent to an effective feature height that is reduced. In fact, the ALM matches the moving position of the peak signal if an effective feature height is used given by

$$h_{eff} = h - R/1.7 \quad (6)$$

The second effect of top corner rounding is the reduction of the peak linescan signal. This reduction makes the position of the top CD less distinct, just as the top CD of the actual feature becomes less distinct in the presence of rounding. The ALM can account for this as an increase in the volume loss factor, α_v . The loss of the corner material provides less interaction volume to generate secondaries, making the peak signal lower. By fitting the ALM to Monte Carlo simulated linescans for a variety of top corner rounding radii, the results shown in Figure 6 were obtained. The impact of top corner rounding on α_v levels off as the radius increases. Also, the largest effect is for a sidewall angle near 80°.

The final effect of top corner rounding that can be observed in Figure 5 is a reduction of the linescan slope corresponding to the inside of the edge bloom of the feature. This has the effect of making an extrapolation to the top as a method of obtaining the top CD less precise. From the perspective of the ALM, the reduction of the slope is equivalent to reductions of both the top forward scatter range and the top volume loss range. Figure 7 shows the ALM parameters as fitted to Monte Carlo results as a function of top corner rounding radius. The step feature volume loss range increases approximately linearly with the top corner rounding radius and is independent of sidewall angle. The step feature's forward scatter range is dependent upon sidewall angle, but that dependence disappears as the corner radius increases. Essentially, as the top corner radius exceeds the forward scatter range, the scattered electrons stop communicating with the sidewall and only depend on the rounded corner shape.

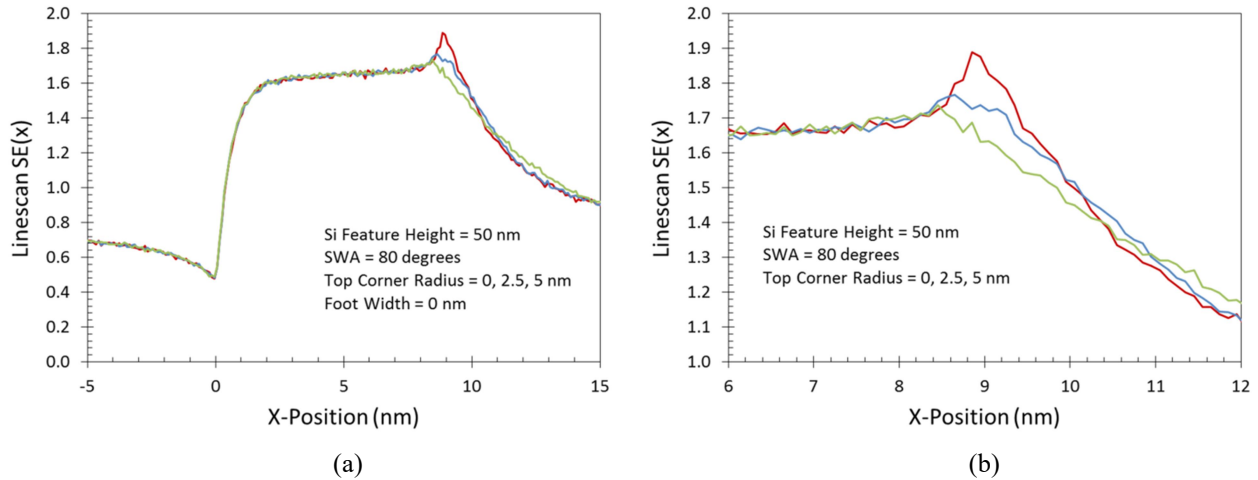


Figure 5. Monte Carlo simulation results showing the impact of top corner rounding of varying radii on the resulting linescan (50-nm tall, 80° silicon edge on a silicon wafer, 500 V, point beam of electrons). The linescans with and without corner are compared in (a) with the region around the peak magnified in (b).

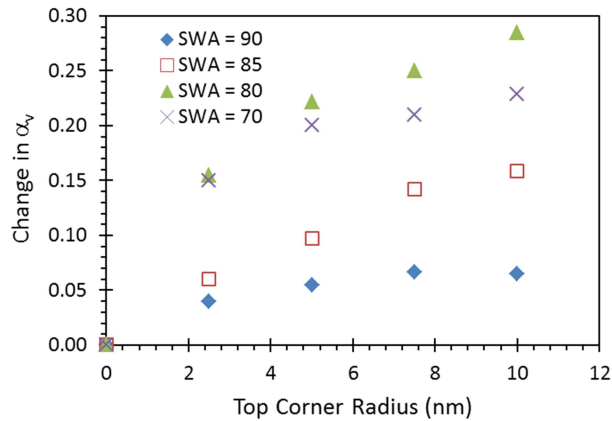


Figure 6. Fitting the ALM to Monte Carlo simulation results allows the step volume loss factor α_v to be correlated with the top corner rounding radius. Here, the change in α_v , compared to no top corner rounding is shown.

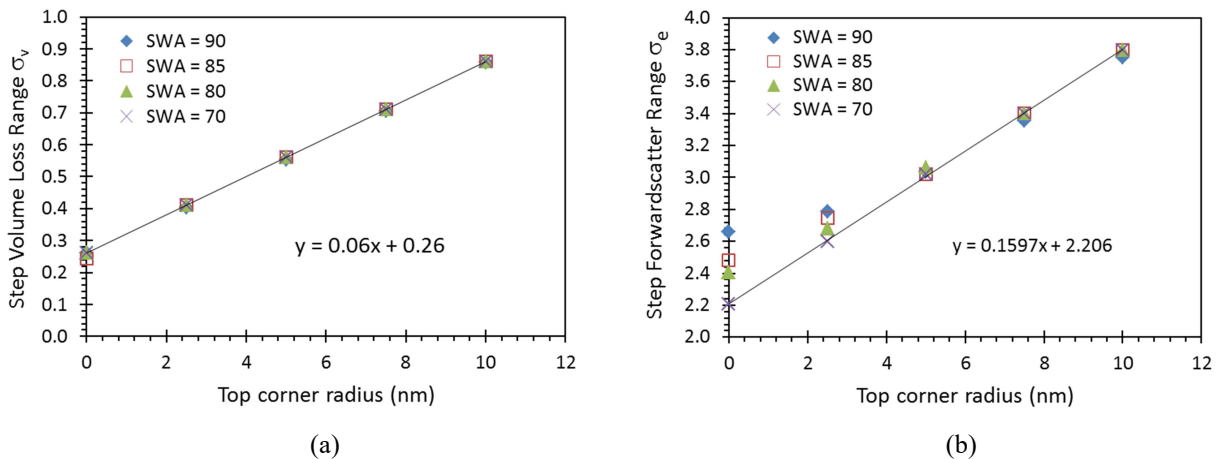


Figure 7. Monte Carlo simulation results showing the impact of top corner rounding of varying radii on two ALM parameters (20-nm tall silicon edge on a silicon wafer, 500 V, point beam of electrons): (a) the feature volume loss range σ_v , and (b) the feature forward scatter range σ_e .

One purpose of adding top corner rounding to the ALM is to see if the ALM can match simulated linescans for sidewall spacer features frequently encountered during self-aligned double or multiple patterning. These features are asymmetric, with one side essentially 90° with a sharp top corner, and the other side sloped (for example, at 80°) and with a rounded corner. Figure 8a shows an example of the geometry used. Figure 8b shows the result of one Monte Carlo simulation and the best fit ALM. Obviously, the ALM is capable of adequately fitting this asymmetric linescan. Further work is required to calibrate the ALM parameters over a wide enough range of conditions to make it predictive for these features.

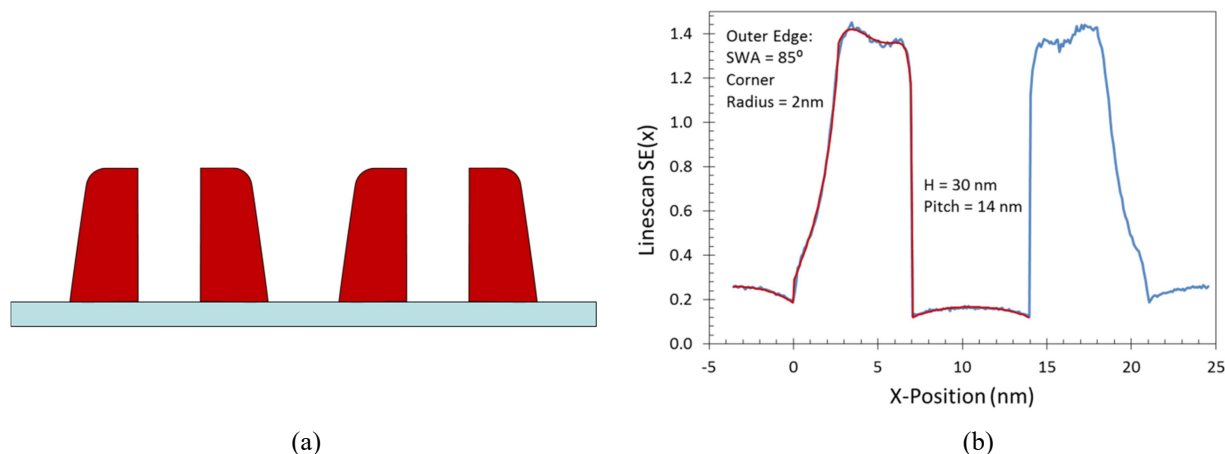


Figure 8. Applying the ALM to sidewall spacer features: (a) an example of a set of asymmetric sidewall spacer features, and (b) Monte Carlo simulated linescans (blue jagged line) with a best-fit ALM (smooth red line). The silicon feature lines and spaces were 7 nm wide at the bottom.

5. Conclusions and Future Work

The analytical linescan model (ALM) that has been developed in this and previous work offers several important advantages. After calibration against a rigorous Monte Carlo simulator for the various materials involved in the sample, the ALM can, with quite reasonable accuracy, predict the linescans of those materials for a wide variety of geometric shapes. In particular, for the case of a 500 eV landing energy, feature thicknesses between 20 and 100 nm, and sidewall angles greater than 45°, the calibrated ALM matches the Monte Carlo simulated secondary electron waveforms over a wide range of feature sizes, pitches, thickness, and sidewall angles. While only silicon features on silicon wafers were tested here, it is expected that similar calibration procedures would yield similar results for a wide variety of materials. Since the model is based on reasonable physical assumptions and uses physically-based parameters, both interpolations and extrapolations to a wide range of geometries should prove possible.

In addition, top corner rounding up to about 10 nm in radius does not require a modification of the form of the ALM, only a change in its parameter values. Footing can also be accommodated, if modeling the fine detail of the foot is not needed. The ALM is applicable not only to symmetrically shaped lines and spaces, but to asymmetric features as well. Still, more work is required to complete the calibration of the ALM over a full range of small features with varying sidewall angles and top corner rounding. Future work will carry out these calibrations with the hope of making the ALM predictive of features such as sidewall spacers used in self-aligned double patterning. Extension to other material sets is also important, as well as exploration of how charging influences the results.

6. Acknowledgements

We would like to thank John Villarrubia of NIST for his writing and continued support of the JMONSEL SEM simulator code, and also for many insightful discussions on its use, on edge detection and model-based algorithms, and CD metrology and simulation studies in general.

7. References

-
- ¹ J. S. Villarrubia, N. W. M. Ritchie, and J. R. Lowney, “Monte Carlo modeling of secondary electron imaging in three dimensions”, *Proc. SPIE*, **6518**, 65180K (2007).
 - ² J. S. Villarrubia, and Z. J. Ding, “Sensitivity of SEM width measurements to model assumptions”, *J. Micro/Nanolith. MEMS MOEMS*, **8**(3), 033003 (2009).
 - ³ J. S. Villarrubia, A. E. Vladár, B. Ming, et al., “Scanning electron microscope measurement of width and shape of 10 nm patterned lines using a JMONSEL-modeled library”, *Ultramicroscopy*, **154**, 15 (2015).
 - ⁴ J. S. Villarrubia, A. E. Vladár, and M. T. Postek, “Simulation study of repeatability and bias in the critical dimension scanning electron microscope”, *J. Microlith. Microfab. Microsyst.*, **4**(3), 033002 (Jul–Sep, 2005).
 - ⁵ B. Bunday, T. Germer, V. Vartanian, A Cordes, A. Cepler, and C. Settens, “Gaps Analysis for CD Metrology Beyond the 22 nm Node”, *Proc. SPIE*, **8681**, 86813B (2013).
 - ⁶ Narender Rana, Yunlin Zhang, Taher Kagalwala, and Todd Bailey, “Leveraging advanced data analytics, machine learning, and metrology models to enable critical dimension metrology solutions for advanced integrated circuit nodes”, *J. Micro/Nanolith. MEMS MOEMS*, **13**(4), 041415 (2014).
 - ⁷ M. P. Davidson and A. E. Vladár, “An inverse scattering approach to SEM line width measurement”, *Proc. SPIE*, **3677**, 640–649 (1999).
 - ⁸ J. S. Villarrubia, A. E. Vladár, J. R. Lowney, and M. T. Postek “Edge determination for poly-crystalline silicon lines on gate oxide”, *Proc. SPIE*, **4344**, 147–156 (2001).
 - ⁹ J. S. Villarrubia, A. E. Vladár, J. R. Lowney, and M. T. Postek, “Scanning electron microscope analog of scatterometry”, *Proc. SPIE*, **4689**, 304–312 (2002).
 - ¹⁰ J. S. Villarrubia, A. E. Vladár, B. D. Bunday, and M. Bishop, “Dimensional metrology of resist lines using a SEM model-based library approach”, *Proc. SPIE*, **5375**, 199–209 (2004).
 - ¹¹ J. S. Villarrubia, A. E. Vladár, and M. T. Postek, “Simulation study of repeatability and bias in the critical dimension scanning electron microscope”, *J. Microlith. Microfab. Microsyst.*, **4**(3), 033002 (2005).
 - ¹² Chie Shishido, Maki Tanaka, and Mayuka Osaki, “Accurate measurement of very small line patterns in critical dimension scanning electron microscopy using model-based library matching technique”, *J. Micro/Nanolith. MEMS MOEMS*, **10**(1), 013010 (2011).
 - ¹³ Benjamin D. Bunday and Chris A. Mack, “Influence of Metrology Error in Measurement of Line Edge Roughness Power Spectral Density”, *Metrology, Inspection, and Process Control for Microlithography XXVIII, Proc.*, SPIE Vol. **9050**, 90500G (2014).
 - ¹⁴ Chris A. Mack and Benjamin D. Bunday, “Analytical Linescan Model for SEM Metrology”, *Metrology, Inspection, and Process Control for Microlithography XXIX, Proc.*, SPIE Vol. **9424**, 94240F (2015).
 - ¹⁵ Carl Georg Frase, Egbert Buhr, and Kai Dirscherl, “CD characterization of nanostructures in SEM metrology”, *Meas. Sci. Technol.*, **18**(2), 510–519 (2007).